Article

Not peer-reviewed version

Multisensor integrated platform based on MEMS charge variation sensing technology for biopotential acquisition

Fernanda Irrera *, Alessandro Gumiero, Alessandro Zampogna, Federico Boscari, Angelo Avogaro, Michele Gazzanti pugliese di cotrone, Martina Patera, Luigi Della Torre, Nicola Picozzi, Antonio Suppa

Posted Date: 31 January 2024

doi: 10.20944/preprints202401.2242.v1

Keywords: Wearable sensors, long-time biopotential recording, MEMS technology, charge variation sensors, low power consumption.

Article

Multisensor Integrated Platform Based on MEMS Charge Variation Sensing Technology for Biopotential Acquisition

Fernanda Irrera [1,*], Alessandro Gumiero [2], Alessandro Zampogna [3], Federico Boscari [4], Angelo Avogaro [4], Michele Gazzanti Pugliese di Cotrone [1], Martina Patera [3], Luigi Della Torre [2], Nicola Picozzi [2] and Antonio Suppa [3,5]

[1] Department of Information engineering, Electronics and Telecommunications, Sapienza University of Rome, Via Eudossiana 18, Roma
[2] STMicroelectronics Agrate, Via Olivetti 2, Agrate Brianza (MB)
[3] Department of Human Neurosciences, Sapienza University of Rome, Viale dell'Università 30, Roma
[4] Department of Medicine, University of Padua, Via Giustiniani 2, Padova
[5] IRCCS Neuromed, Via Atinense 18, Pozzilli (IS)
* Correspondence: fernanda.irrera@uniroma1,it.

Abstract. We propose a new methodology for long-time biopotential recording based on MEMS multisensor integrated platform featuring a commercial electrostatic charge transfer sensor. That family of sensors was originally intended for presence tracking in automotive, so the existing setup has been engineered for the acquisition of electrocardiogram, electroencephalogram, electrooculogram and electromyography, designing a dedicated front-end and writing a proper firmware for the specific application. Systematic tests on controls and nocturnal acquisitions from patients in domestic environment will be discussed in detail. The excellent results candidate this technology to provide a low power, unexplored solution to biopotentials acquisition. The technology breakthrough is in that it enables adding this type of functionality to existing MEMS boards at near-zero additional power consumption. For these reasons, they open to additional possibilities for wearable sensing and strengthen the role of MEMS technology in medical wearable applications for long time synchronous acquisition of a wide range of signals.

Keywords: wearable sensors; long-time biopotential recording; MEMS technology; charge variation sensors; low power consumption

1. Introduction

In the near future, wearable technologies will be pervading medical areas [1]. Ubiquitous monitoring and remote supervision make wearables extremely appealing for clinicians, making instrumental exams accessible in domestic environments. Among others, this is the case of electroencephalogram (EEG), electrocardiogram (ECG) and electromyography (EMG), on which research is spending great efforts to provide wearable variants [2–4],

EEG is usually performed by trained personnel in ambulatory settings, recording several channels by placing numerous electrodes across the scalp with cables connecting to instrumentations, thus resulting in a lengthy and uncomfortable setup procedure. Although this analysis provides fundamental and exhaustive insights into a variety of disorders, not always this is the best way to obtain the desired information from the EEG. Indeed, in specific circumstances or for certain diseases, it would be preferred to monitor even just one channel EEG, but continuously for several days, in a domestic environment and free-living conditions, rather than several channels for short time in hospital. For example, this is the case, of re-enabling communication through brain-computer interface approaches in patients suffering from advanced stages of paralyzing disorders, such as amyotrophic lateral sclerosis (ALS) [5]. Today, portable EEG devices are also available, but their bulkiness, obtrusive setup, and limited battery life underscore the need for a wearable technology

 doi:10.20944/preprints202401.2242.v1

offering both prolonged and comfortable monitoring, which is more crucial than obtaining multiple channels. Moreover, by providing real-time, long-term and free-living dynamic information, new non-invasive wearable solutions for EEG monitoring would support the differential diagnosis of pathological conditions characterized by transitory changes in focal brain activity, including epileptic and non-epileptic disorders, such as the loss of consciousness (i.e., cardiovascular syncope) and parasomnias (i.e., REM behaviour disorder) [6,7]. To testify the importance of portability, in the last few years, several portable EEG devices have appeared on the market [8–16], including in-ear EEG sensors [17,18]. However, none of these devices has successfully addressed the dual challenge of providing a battery lifespan longer than 12 hours and ensuring sustained comfort for prolonged in-home applications.

Regarding ECG, it is noteworthy that that this analysis encounters similar challenges to EEG relatively to the test environment, comfort and duration. Indeed, a comprehensive monitoring over several days is essential for diagnosing paroxysmal arrhythmias, evaluating potential arrhythmic symptoms and understanding syncope mechanisms [19]. ECG holters, which usually acquire information for up to 48 hours, often fail to identify heart rhythm disturbances due to limited monitoring duration [20].The likelihood of identifying an arrhythmia like atrial fibrillation notably increases with extended monitoring, carrying substantial therapeutic implications [21]. Indeed, to prolong monitoring durations of cardiac activity, a "loop recorder" is occasionally adopted. However, this solution demands the invasive subcutaneous implantation of a device, thus limiting its widespread application. Unfortunately, most commercially available wearable systems are either limited in their recording sessions (the recording automatically stops after 30-300s and has to be restarted) or in their battery life, preventing continuous monitoring for durations exceeding 24 hours [22].

When considering EMG, its importance is evident in cases where monitoring muscle activity and distinguishing between involuntary and voluntary muscle contractions are crucial, such as in specific movement disorders associated with neurological diseases. Surface EMG (sEMG) uses patch electrodes and is not invasive, offering greater comfort and tolerance for patients compared to needle-based EMG. Moreover, the capability for multichannel operation allows the acquisition of signals from multiple muscles simultaneously [23,24]. Traditionally, sEMG is performed within healthcare facilities using wired equipment, presenting several challenges. Firstly, these tests are usually short-lasting and conducted in non-domestic environments, thus not truly representative of clinical conditions. Secondly, the presence of wires imposes spatial constraints on patients, restricting their range of movements. Furthermore, the wired connection to the electrical grid introduces noise at 50 Hz, which coincides with a crucial segment of the EMG spectrum in many tests. To overcome these limitations, in recent years wireless wearable sEMG devices have been proposed for use in a very wide horizon of applications, and some products are already on the market (see, for example, [25–28]). However, also for wearable sEMG systems, applications are limited by the short battery life. Indeed, a comparison of products on the market shows that the lowest power consumption is some tens of mW, resulting in battery lifespans of less than 8 hours [29–32]. Very recently, a s-EMG system has been presented in literature, that supports high sampling and lower power consumption measurement [33]. This innovative approach optimized each part of the EMG acquisition circuit and combined an MCU with BLE for transmission to a smartphone. By employing a smart signal management strategy, the authors claim an extended battery life longer than that of commercial devices.

In summary, despite the clinical importance of recording data over extended periods, current commercial wearable ECG, EEG and EMG devices show limited battery life, typically lasting 24 hours for ECG, 12 hours for EEG and even less for EMG. These energy limitations are in conflict with the envisioned days or weeks of monitoring and do not allow space for future developments. Indeed, the existing constrains in processing power and device battery life not only preclude the integration of sophisticated machine learning algorithms [34] but also make it unfeasible to directly embed artificial intelligence on the boards. In addition, the energetic constrains limit the capacity to acquire a broader spectrum of information, including synchronously-recorded biopotentials along with other

 doi:10.20944/preprints202401.2242.v1

physical or physiological parameters using a single device - a potentially valuable diagnostic approach in many cases. Long time monitoring, polygraphic recording and smart algorithms embedding at the same time, would represent a breakthrough for many applications in medicine. With such an overview, it is clear that new strategies and technologies are necessary to reduce the power consumption of wearable sensing systems and improve their functionality and versatility.

In this context, we propose a commercial MEMS multi-sensor integrated system featuring a charge transfer sensor (QVAR), designed for long-time recording of biopotentials and inertial data. Originally developed for presence tracking in automotive, we innovatively engineered the QVAR sensor to adapt the existing setup to biopotential acquisition, designing a dedicated front-end and writing a proper firmware. This technology provides an incredibly low power, unexplored solution to biopotentials acquisition, and also enables adding this type of functionality to any existing MEMS board at near-zero additional power consumption (< 20 ◎A per channel). For these reasons, QVAR sensors open to additional possibilities for wearable sensing and strengthen the role of MEMS technology in medical wearable applications for long-time synchronous acquisition of ECG, EEG, EOG, sEMG and inertial signals. To our knowledge, this is the first time that an electrostatic sensor based on electric charge transfer is used for health applications.

2. Materials: The QVAR sensor

2.1. Operation principles

The focus of this paragraph is the QVAR sensor, an electrostatic charge variation sensor. It is commonly incorporated into MEMS chips that are manufactured by STMicroelectronics. Usually the QVAR analog front-end (AFE) is combined with a finite state machine (FSM) and a machine learning core (MLC). This combination allows outstanding edge processing capabilities. The QVAR evaluation board is depicted in Figure 1a. The electrostatic sensors are usually used to detect a charge variation on a surface induced by another object. QVAR with its differential input can detect electrical potential variation induced over the two electrodes. It is used in various applications such as presence detection, touch sensing and user interface creation.

The QVAR is available in a small thin plastic land grid array package (LGA) and it is guaranteed to operate over an extended temperature range from -40 °C to +85 °C.

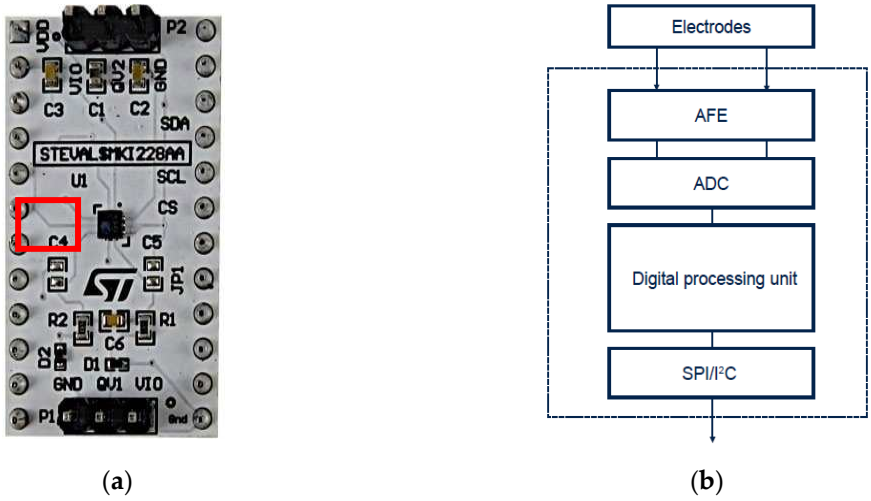

(**a**) (**b**)

Figure 1. (a) QVAR evaluation board details: the sensor is highlighted by the red box**; (b)**. High level QVAR block diagram and electrodes**.**

This functionality enables the detection of changes in BIO potential with the addiction of minimal electronics required to condition the inputs. The conditioning process is essential to polarize the electrodes and amplify the overall gain of the acquisition chain based on the signal being

 doi:10.20944/preprints202401.2242.v1

analyzed. Electrode polarization helps prevent saturation that may be caused by the body's coupling with external potential originating from electromagnetic disturbances.

Eventually the QVAR allows a very simple, low cost and low power vital signs reading. QVAR offers high performance and ultralow power for long battery life. The AFE channel has low noise, high common-mode rejection ratio (CMRR) as well as programmable gain and input impedance.

In Figure 1b the block diagram of a the QVAR sensing channels is sketched. The blocks are:

1. Electrodes: the electrodes are always necessary to read the signals. Usually they are made of copper, silver, tin, gold and can change in dimensions. It is important to reduce at minimum the series resistance introduced by electrodes, but the high input impedance of the QVAR helps in the choice.
2. AFE: it is an Analog Front-End which realizes the conditioning and the amplification. External amplification is not always necessary.
3. ADC: it is a 12-bits analogic to digital converter
4. Digital Processing Unit: it is composed by Finite State Machine and Machine Learning Core

2.2. Electrical Features

As previously mentioned, QVAR is typically integrated into pre-existing MEMS devices that serve various functions. This integration is highly advantageous in many cases. For instance, it enables the simultaneous acquisition of BIO electrical signals and motion information, which is crucial in correcting artifacts, without the need for complex electronics or increased power consumption.

In Table 1 and Table 2 typical values of the principal electrical parameters and characteristics of the QVAR have been reported at VDD=1.8 V and room temperature, respectively.

Table 1. Typical values of the principal electrical parameters of the QVAR at VDD=1.8 V and 25°C.

Electrical Parameters @ VDD = 1.8 V, T = 25 °C	**Typ.**
Supply voltage	1.62 V to 3.6 V
I/O pins supply voltage	1.62 V to 3.6 V
Current consumption	50 ◎A
Current consumption in power-down	2.1 ◎A
Digital high-level input voltage	0.7*VDDIO
Digital low-level input voltage	0.3*VDDIO
Digital high-level output voltage	VDDIO - 0.2 V
Digital low-level output voltage	0.2 V

Table 2. Typical values of the principal electrical characteristics of the QVAR at VDD=1.8 V and 25°C.

Electrical Characteristics @ VDD = 1.8 V, T = 25 °C	**Typ.**
ODR (Configurable output data rate)	800 to 3200 Hz
Input range (DC coupled)	±25 to ±200 mV
Offset (Input referred)	±1 mV
Noise Shorted input, gain 16, BW 20 ÷ 400 Hz, input referred	10 uV_{RMS}
ADC gain (Gain = 16, input referred)	1311 LSB/mV
Channel gain (Configurable)	2 to 16 V/V
Input common mode	0.61 V
CMRR 50 Ω input source, sinus. input 100 mVp@50 Hz, gain 2	80 dB
Input impedance (Configurable)	100 to 1000 MΩ
Bandwidth (Configurable)	50 to 1600 Hz
ADC resolution	12 bit

 doi:10.20944/preprints202401.2242.v1

2.3. Potentiality and limits of the QVAR sensor

Currently, QVAR provides an optimal and easily integrated solution for simultaneously performing different readings of biopotentials and inertial parameters. This is achieved while maintaining the energy consumption and cost of the final solution almost unchanged.

Unlike signals such as ECG, EMG and EOG, for the acquisition of EEG signals the actual QVAR requires the use of external amplification to detect those weak electrical signals. Increasing the gain of the internal chain and improving the performance in terms of input noise and CMRR would easily solve this need. It would also provide greater immunity to external disturbances, potentially allowing the system to operate without a third reference electrode to polarize the human body during measurement.

New versions of the QVAR are currently being developed by STMicroelectronics which can guarantee, in addition to the above-mentioned requirements, also a greater input impedance. This allows for a better transfer of signals from the electrodes to the acquisition chain, making it possible to use dry electrodes for measurements. With these improvements, QVAR can potentially acquire any type of biopotential without the need for external electronics and reference electrodes.

3. Methods: biopotential acquisition by QVAR

3.1. Acquisition of ECG

To record the ECG signal with the QVAR, we used a single-lead ECG setup and determined the heart frequency by detecting the R-peaks and the evaluation of RR intervals. Specifically, a lead D1 configuration, placing positive and negative electrodes on the left and right upper extremities, respectively, was adopted. Wet Ag/Cl electrodes were positioned in RA-LA configuration within the Eindhoven triangle, as illustrated in Figure 2 [35] and the trace was recorded for an extended duration (i.e., tens of seconds). The signal underwent filtration in the 1-35 Hz band. Additional details on the technique of ECG recording with QVARs can be found in [36]. An illustrative example of a single ECG oscillation recorded with QVAR is presented in Figure 3. Notably, typical features such as the P wave, QRS complex, and T wave are distinctly recognizable [37]. The extraction of RR intervals between consecutive oscillations allows the calculation of the hearth rate (HR). Another clinically significant metric which can be obtained from that trace is the QT length and its normalized value (i.e., $QT_C = QT/RR^{1/2}$). In multi-channel ECG acquisitions, variations in electrode locations change the morphology of the ECG waveform. However, the R-peak period and consequently the length of RR intervals remain independent of the chosen derivation. Accordingly, the HR measurement derived from RR intervals is derivation-independent [38].

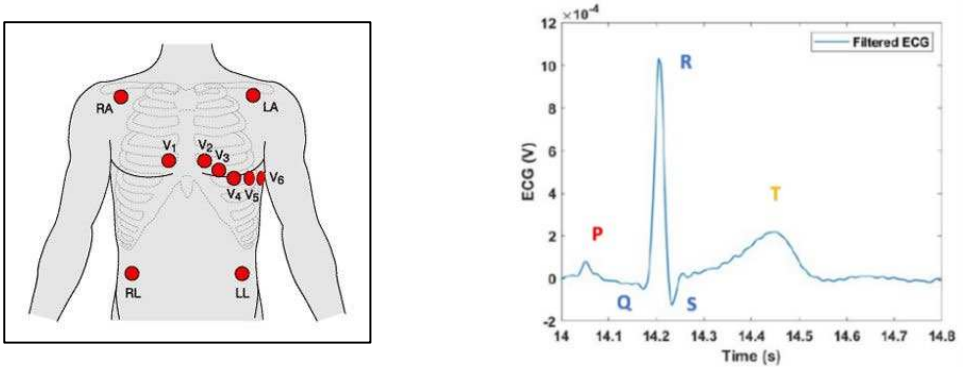

(**a**) (**b**)

Figure 2. (a): Electrode placement for a 12-lead ECG configuration, with electrodes on right arm (RA), left arm (LA), left leg (LL), right leg (RL) and chest electrodes V1 to V6. (b): Zoom of a single oscillation recorded by the QVAR sensor with two electrodes in the RA-LL configuration.

Preprints.org (www.preprints.org) | NOT PEER-REVIEWED | Posted: 31 January 2024 doi:10.20944/preprints202401.2242.v1

To prove the robustness of our sensing technique with respect to the derivation, we conducted a simultaneous acquisition using both the QVAR and a gold standard system (the certified Micromed system) positioning electrodes in distinct configurations. Referring to Figure 2, we adopted the RA-LA configuration for the QVAR system and the RA-LL configuration for the gold standard. In Figure 3 both traces are presented, with dashed vertical lines added for clarity to highlight the R peaks. Notably, the R peaks from the QVAR system are perfectly synchronized with those from the gold standard, despite the adoption of different derivations. Based on the use of a single-lead ECG, our approach would be suitable for a basic heart monitoring of rhythms, enabling the detection of arrhythmias, such as atrial fibrillation, and the examination of pathologic HR variability (HRV) [39].

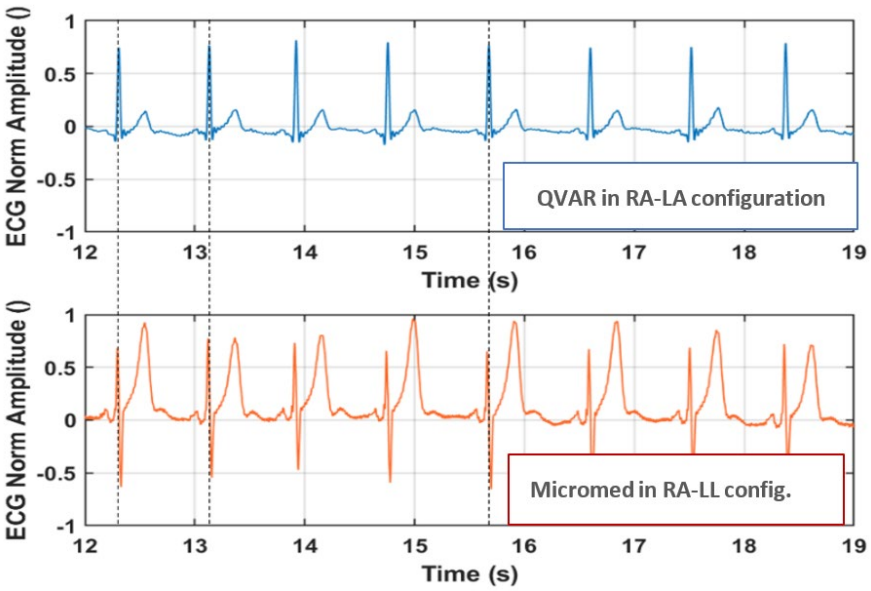

Figure 3. Normalized ECG trace acquired simultaneously by the QVAR and MicroMed systems, from RA-LA and RA-LL configurations, respectively. Dashed lines highlight the R peaks.

3.2. Acquisition of EEG and EOG

We simultaneously acquired a single-channels EEG using both QVAR and a gold standard system (Micromed or the Cyton- BCI). As a first test, we placed the electrodes on the frontal lobes at locations Fp1-Fp2, following the International 10-20 System Standard [40]. To ensure comparability, the electrodes of the gold standard (Micromed) and QVAR were positioned as closely as possible, as discussed in [36]. During this setup, the subject was instructed to keep his eyes closed to record brain activity. The raw traces from a short interval are shown in Figure 4: the blue line refers to the QVAR recording, while the red trace to the gold standard recording. Notably, the two traces overlap significantly. The peak at 61 seconds, recorded by both systems, corresponds to a blinking event.

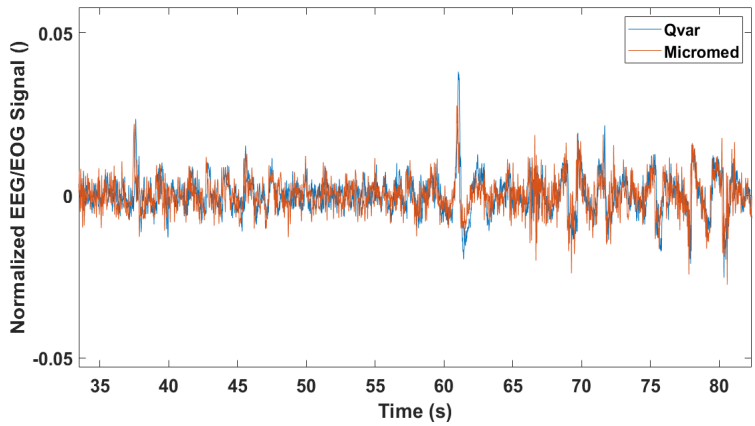

 doi:10.20944/preprints202401.2242.v1

Figure 4. Raw traces of single-channel EEG acquisition from frontal lobes by Micromed and QVAR.

The electro-oculogram (EOG) derives from an artefact in the frontal channels of the EEG [41], which allows to detect eye blinking and movements and can be useful in specific medical areas [42, 43]. One of the main applications of EOG is sleep staging [44]. Indeed, the so-called "rapid eye movement" gives the name to REM sleep phase itself. Optimizing EOG detection involves filtering the raw trace acquired from frontal electrodes (Fp1-Fp2) within a specific frequency band. So, in the following test, a subject was instructed to perform various random eye movements, including blinking and rotations. In Figure 5, the 1-3 Hz filtered and normalized traces of both QVAR and gold standard system (Cyton BCI) are presented. The comparison reveals an excellent agreement between the two traces.

Electrodes placed in occipital sites, namely O1 and O2 following the International 10-20 System Standard, and filtered within the 8-13 Hz band, maximize the contribution of ◎ waves. Figure 6 displays the normalized filtered traces of QVAR and the gold standard (Cyton BCI) during a test where the subject remained relaxed with eyes closed. The typical fusiform pattern is distinctly visible, with approximately ten peaks in each fuse. Once again, the agreement of the two traces is excellent.

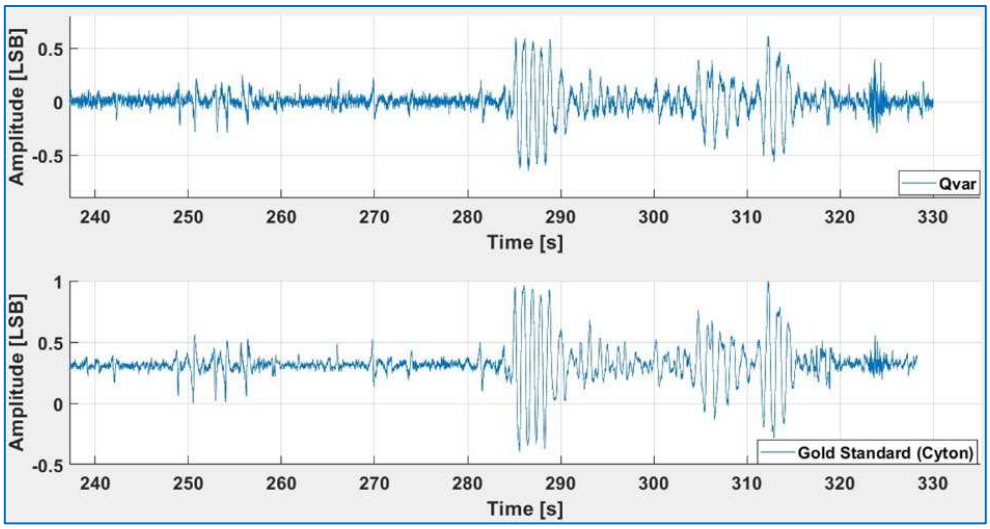

Figure 5. 1-3 Hz filtered normalized signal acquired in FP1-FP2 with QVAR (top) and gold standard (bottom) during random mixed eyes actions.

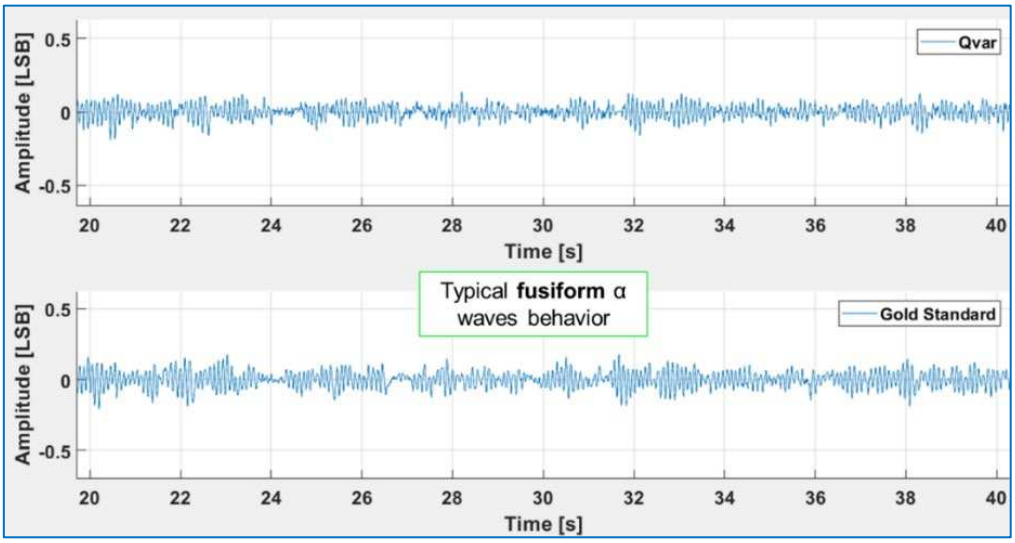

 doi:10.20944/preprints202401.2242.v1

Figure 6. 8-13 Hz filtered normalized signal acquired in O1-O2 with QVAR (top) and gold standard (bottom) with closed eyes.

3.3. Acquisition of sEMG

Wearable sEMG has found widespread commercial applications ranging from gaming to rehabilitation medicine, analysis of motion, analysis of muscle fatigue, and prosthesis control. Less popular applications span from drowsiness control in car drivers [45], the study of hand gestures reproducing sign language [46], monitoring involuntary activity of the jaw muscles [47], and analyzing facial expression [48]. In the mentioned applications, the sEMG signal amplitude depends from the specific muscle under study and the type of activity, which, rarely, is higher than few millivolts. On the contrary, the power spectrum of a typical raw EMG signal has consistent frequency components irrespective of the muscle being examined or the type of physical connections (needles or patch electrodes). The band of interest consistently falls between 3 and 500 Hz, with the primary content concentrated between 10 and 250 Hz. Conventionally, this analysis is performed during outpatient visits by means of wired research laboratory equipment. It involves three electrodes properly placed on the skin, with positive and negative electrodes positioned over the target muscle and a third reference electrode placed at a distance from it.

In our experiments, we focused on two distinct muscles, namely the flexor carpi radialis and the facial masseter, which are characterized by a very different conformation and activation intensity. The experimental protocol involved the subject performing few times the following simple sequence: 5" contraction followrd by 5" relaxation, starting from a relaxed condition. To validate the test, the exercises were conducted with the subject concurrently wearing the QVAR wearable device and the EMGClick by MiKroElectronika, a commercial wearable device, established as the gold standard [49]. The primary objective of the test was to ensure that the QVAR device accurately detected muscle activation without generating false activations. This test is of the type ON/OFF, without any intensity evaluation. The collected signals underwent the following processing steps: 1) HP filtering at 3 Hz to remove DC and movement artifacts, along with notch filtering at 50 Hz; 2) rectification; 3) smoothing with LP filtering at 10 Hz to hold on the envelope; 4) normalization. Each experiment was systematically repeated by inverting the position of the QVAR and EMGClick electrodes, in order to verify the independence of results on electrode placement. In Figure 7, the patch electrodes positioned on the arm to test activity of the flexor carpi radialis are depicted. The black and white electrodes belong to the QVAR device, while the others pertain to the gold standard, including the reference electrode on the wrist. In the same figure, two traces are displayed: the one collected by the QVAR (top) and the one collected contemporarily by the EMGClick (bottom). As one can see, the QVAR precisely reports muscle activity, demonstrating exact synchronization with the gold standard within a fraction of second.

Regarding the acquisition on the masseter, as illustrated in Figure 8, patch electrodes on the face were employed to test activity of the masseter. Again, the black and white electrodes belong to the QVAR device, while the others belong to the gold standard, which includes the reference electrode on the neck. The displayed traces show a clear and synchronous recording of muscle activity by the QVAR (top trace) and EMGClick (bottom trace).

As a final remark, it is noteworthy that that this is the first reported application of QVAR for sEMG recording.

 doi:10.20944/preprints202401.2242.v1

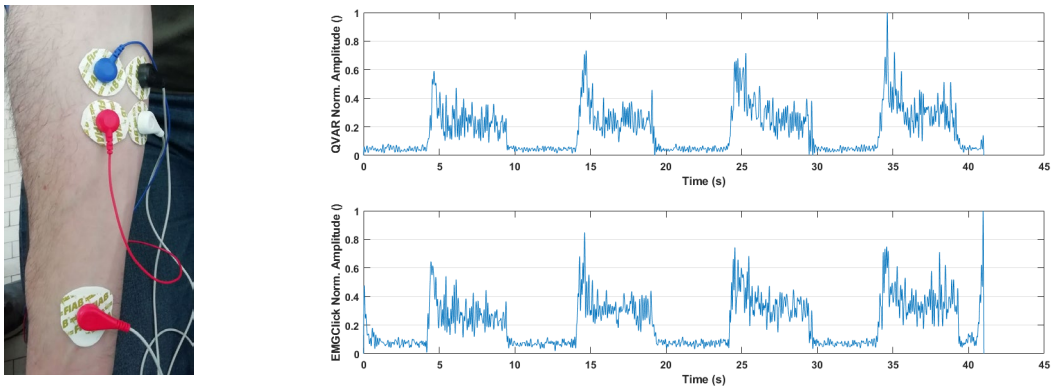

(**a**) (**b**)

Figure 7. Picture of the patch electrodes positioned on the flexor carpi radialis. The traces collected by QVAR (top) and the EMGClick (bottom) are displayed by the side.

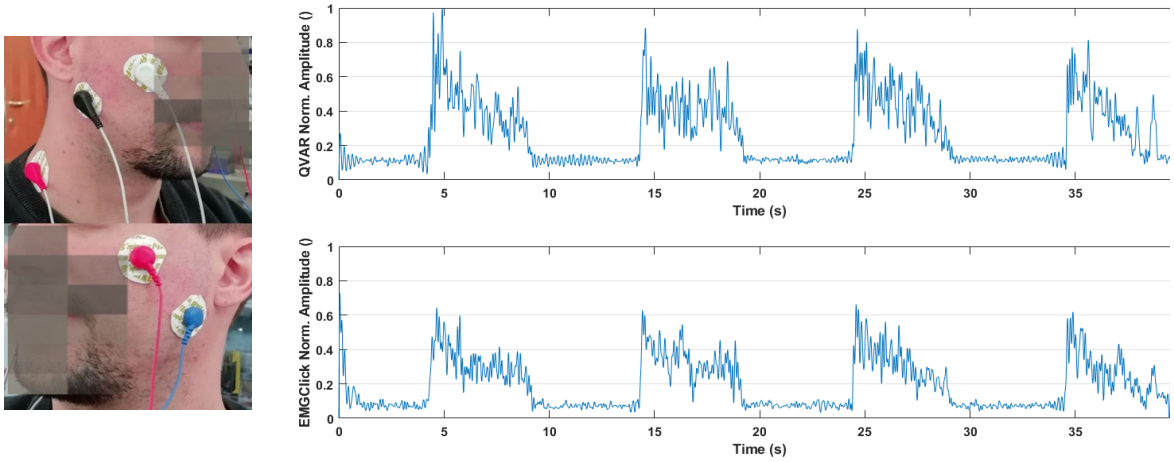

(**a**) (**b**)

Figure 8. Picture of the patch electrodes positioned on the masseter. The traces collected by QVAR (top) and the EMGClick (bottom) are displayed by the side.

4. Discussion: two case studies

4.1. Domestic monitoring of vital signs in hypoglycemia

Diabetes is a metabolic disorder characterized by high blood glucose that affects, today, around half a billion persons worldwide, with an estimated year cost of 10% of the global health expenditure. Type 1 diabetes (T1D) is due to insulin deficiency and is treated pharmacologically by insulin administration, which in any case cannot replicate the physiological secretion and thus leads to glucose oscillations. Hypoglycemia (HG) is a major threat in T1D patients and commonly occurs in clinical practice as approximately 90% of all patients who receive insulin [50]. In average, individuals with T1D experience about two episodes of symptomatic hypoglycemia per week. The prevalence of severe hypoglycemia, which necessitates assistance for recovery, is approximately 30-40% annually, with an incidence of 1.0-1.7 episodes per patient per year. The likelihood of experiencing this risk increases considerably with prolonged disease duration [51]. Symptoms of hypoglycemia can be mainly divided in two categories: neurogenic (autonomic) and neuroglycopenic. Neuroglycopenic symptoms are caused by brain glucose deprivation and include cognitive impairment (altered perception, poor concentration, slow speech, slow decision-making), behavioral changes (irritation, frustration), psychomotor abnormalities (weakness, incoordination), seizure/coma and permanent

 doi:10.20944/preprints202401.2242.v1

neurological damage for prolonged severe hypoglycemia [52]. Neurogenic symptoms on the other hand are caused by the sympathoadrenal response and include adrenergic symptoms (palpitations, tremulousness, anxiety, arousal, skin pallor/flushing or blotchy rashes, tingling around the mouth/lips) and cholinergic symptoms (sweating, hunger, paresthesia) [52].

Nocturnal HG is particularly dangerous because symptoms are typically blurred by sleep, sometimes resulting in coma and even death. It is known that during the transition to HG, in order to bring blood sugar level back up to normal, the body elicits a hormonal response which in turn leads to a number of symptoms. These include heart rate variability, progressive degradation of cognitive functionality and cerebral activity.

To get deeper insight into evolution of vital signs during transition to HG condition, we propose a wearable system based on QVAR sensors recording electrocardiogram and electroencephalogram during the night, for use in domestic environment. The strategy would be to correlate those biopotentials to the level of glucose in blood measured instantaneously by a glucose sensor. Some authors identified a meaningful set of parameters to be extracted from ECG and EEG traces in time and in frequency domains, that have been observed to alter before the onset of a HG episode. From ECG, they focused on the QT_c interval length, the RR tract, the HR and the HRV with its standard deviation normal to normal (SDNN) and its root mean square (RMSSD) and, finally, the low/high-frequency ratio (LF: HF) of the HRV power spectrum [53–61]. Regarding the EEG, only few authors reported results starting from the power spectrum of ⍵-waves and calculating the frequency centroid CF (and the spectral rotational radius derived from spectral moments G0 and higher) [62–64].

The hardware of our system consists of two boards, each integrating a Qvar sensor, a microcontroller, a battery, a microSD memory. The two boards are fixed on the chest: one sensor acquires ECG with two electrodes in RA-LA positions, the other sensor acquires the ⍵-wave EEG with two electrodes on the occipital sites O1 and O2. Data are all stored in the microSD. Preliminary verification of the correct operation of the QVAR system was performed on control subjects, by comparison with a gold standard (Cyton BCI, in this case). Table 3 summarizes values of the parameters calculated from ECG and EEG averaged in 24-hour acquisition on six control subjects: as one can see, the agreement is excellent, with a discrepancy lower than 1.5%.

In Figure 9 the RR trait duration extracted from ECG with our system (top) and the gold standard (bottom) are compared in time and frequency domain. In the same figure, the ⍵-wave ECG recorded with our system (top) and the gold standard (bottom) are compared in time and frequency domain.

Table 3. Values of main ECG/EEG parameters averaged in 24 hour acquisition on six control subjects.

ECG/EEG parameters	Qvar system	Gold standard	Discrepancy %
QTc (ms)	329	334	1,4
RR (ms)	948,4	957,6	0,95
SDNN	149,9	149,1	0,5
LF:HF	0,595	0,590	0,84
CF (Hz)	102,13	102,28	0,1

Preprints.org (www.preprints.org) | NOT PEER-REVIEWED | Posted: 31 January 2024 doi:10.20944/preprints202401.2242.v1

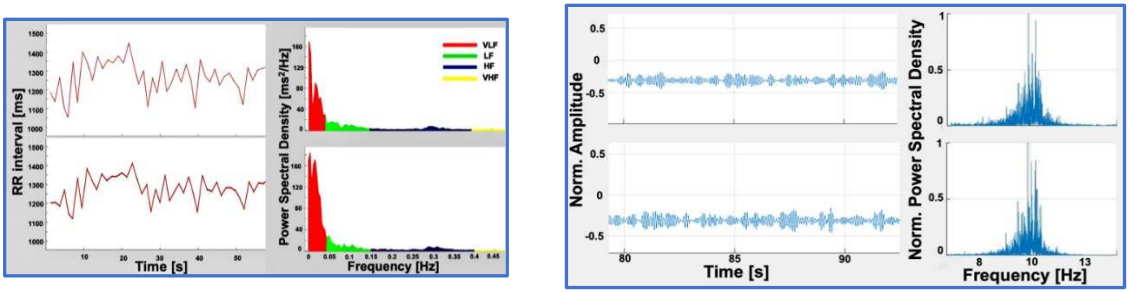

(**a**) (**b**)

Figure 9. Left: RR trait duration obtained with Qvar (top) and the gold standard (bottom) and power spectral density. Right: ◎-wave EEG recorded by Qvar (top) and the gold standard (bottom) and normalized power spectral density.

After those preliminary tests, a T1D patient was studied overnight in domestic environment. He was male, 63 years old, diagnosed at 22, treated with insulin pump and a glucose target value of 120 mg/dl (this relatively high value should not surprise, since each diabetic patient has a specific glucose reference value and a specific hypoglycemia threshold). The patient always puts on a glucose sensor (GS) on an arm, recording the glucose value every minute, whose hypoglycemic alarm is set at 80 mg/dl. The patient gave informed consent to be tested with our device. So, throughout testing nights, he was wearing the QVAR system in addition to the gold standard and the GS. At a certain time (which hereafter will be referred to as t=0), the glucose reached the critical threshold and the GS alarmed the patient, who woke up and immediately assumed sugar. In Figure 10 and in Figure 11 we show values of the ECG parameters (LF:HF, SDNN) and EEG parameter (CF) reported by the QVAR system and the gold standard before the alarm (orange curves). In the same figures, the glucose data recorded by the GM are also drawn with blue solid line. The intervals where ECG and EEG parameters underwent meaningful variation are highlighted with pink shadows and the trends are indicated with dashed lines.

As one can see, the ECG underwent a slow and progressive variation long before the glucose approached the critical value (approximately 90 minutes before, when the glucose decreased below the value of 100 mg/dl), while the ◎-wave EEG exhibited a sudden variation only 15 minutes before the alarm.

At this stage, any conclusion from the clinical viewpoint would be meaningless, since would require much further study and many more patients (beyond the target of this paper), but, on the contrary, the technological conclusion is that our wearable system using QVAR sensors can efficiently monitor simultaneously ECG and EEG channels, allowing to study vital signs before and during nocturnal HG crisis, in domestic environment.

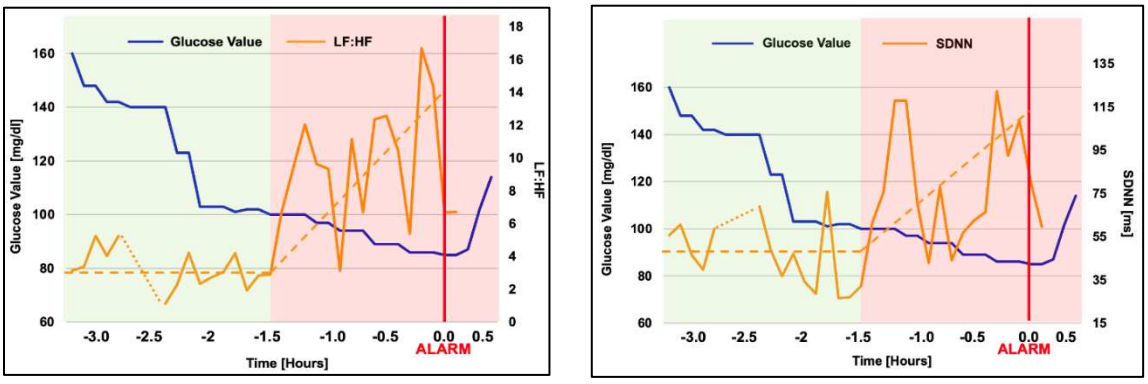

(**a**) (**b**)

 doi:10.20944/preprints202401.2242.v1

Figure 10. Values of the ECG parameters (LF:HF, SDNN) displayed before the alarm (t=0). In the same figures, the glucose data recorded by the GM is also drawn with blue solid line. The dashed line indicates the trends of variation of the studied parameters.

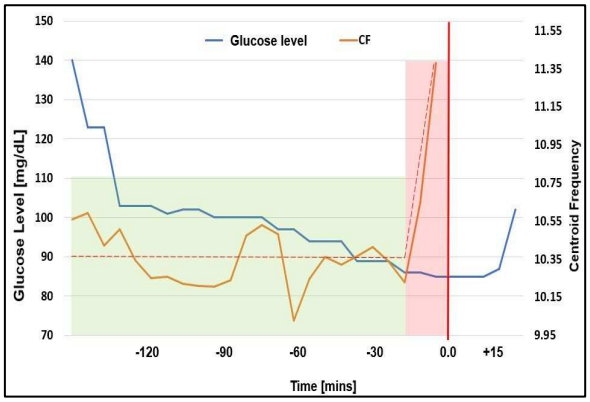

Figure 11. Values of the EEG parameter (CF) displayed before the alarm (t=0). In the same figure, the glucose data recorded by the GM is also drawn with blue solid line. The dashed line indicates the trend of variation of the studied parameter.

4.2. Domestic monitoring of non-EEG biopotentials for REM/NREM sleep screening

Sleep can be disrupted by various disorders that are classified based on the stage of sleep during which they manifest (i.e., rapid eye movement - REM and non-rapid eye movement – NREM sleep phase). These disorders exhibit distinct pathophysiological mechanisms and prognosis, and require specific therapeutic interventions [65]. Accordingly, accurate diagnosis and treatment of different sleep disorders crucially depends on the ability to properly differentiate between sleep phases. One notable example is REM Sleep Behavior Disorder (RBD), a parasomnia occurring during the REM sleep stage, particularly significant for neurologists, psychiatrists, and geriatricians. Indeed, RBD is acknowledged as a precursor to neurodegenerative diseases such as Parkinson's disease, dementia with Lewy body and multiple system atrophy [66,67]. Manifesting as dream enactment behavior [66], patients with RBD engage in activities like screaming, speaking, falling, and mimicking dream motions, often resulting in injuries and violence.. The diagnosis of RBD is usually challenging, necessitating a history of complex sleep behaviors confirmed during REM sleep. REM sleep should be therefore demonstrated, with the contemporary absence of atonia by evidencing dream enactment behavior [68]. The gold standard for the diagnosis of sleep disorders is polysomnography (PSG), according to the American Association of Sleep Medicine (AASM) scoring guidelines. However, PSG is a cumbersome test available in (a very limited number of) medical centers, requiring specialized supervision and leading to prolonged waiting times. Indeed, access difficulties to the PSG contribute to undiagnosed and untreated sleep disorders, with significant consequences. Moreover, it is demonstrated that the environment influences the sleep quality [69], so that the PSG itself may result distorted by the altered emotional state of the hospitalized subject. Accordingly, the challenge with diagnosing RBD extends beyond the need for hospitalization to conduct PSG. Indeed, even after the test is performed, it may result not effective since symptoms do not always appear, necessitating extended hospital stays for an accurate diagnosis. As a consequence, RBD still remains largely undiagnosed [70], like many other sleep-related disorders. Since RBD may precede specific neurodegenerative diseases by several years, recognizing it becomes crucial for identifying at-risk patients during a preclinical phase. The early identification of individuals at risk for neurodegenerative disorders would allow the development and administration of novel neuroprotective drugs, potentially delaying or preventing the onset of specific diseases [71].

Due to all these factors, the field of telemedicine is currently focusing on more widespread screening and home monitoring approaches for sleep disorders [69,72,73]. The aim is to support clinicians in their diagnostic procedures. Domestic screening facilities would play a crucial role in

 doi:10.20944/preprints202401.2242.v1

identifying individuals at-risk who really and urgently need hospitalization for the diagnosis, thus optimizing the utilization of limited PSG resources and the expertise of trained personnel. This approach would reduce waiting times from recognition to diagnosis and treatment of sleep disorders, ultimately increasing adherence to treatment, despite a growing number of sleep consults [74,75]. In the last few years, portable solutions and systems for domestic screening, detecting and/or remote monitoring sleep have been proposed. These can be categorized into two main categories: those using EEG and those that do not.

As mentioned earlier, PSG provides the most accurate and comprehensive insights into sleep patterns. It identifies the REM stage by detecting epochs characterized by low-amplitude, mixed-frequency EEG, low chin/masseter EMG tone and rapid eye movements [76]. On the opposite side, we find examples of extremely less accurate wearable devices, as the commercial sleep trackers (CST), which do not use EEG and focus on fitness rather than on healthcare. These devices rely on measuring the heart rate (HR), HR variability (HRV) and movements using photoplethysmography (PPG) and inertial sensors. While they can distinguish between wake and sleep phases [77–85], they are totally unaffordable for comprehensive analysis of sleep [86-88]. With this information, it is clear that HR, HRV and movements are not fully representative of the REM phase. Using artificial intelligence (AI) can probably increase accuracy of REM staging when the set of data collected is not exhaustive, as demonstrated by some authors [89–92]. However, it is essential to consider that these studies are still at a preliminary stage.

In summary, PSG is the gold standard and EEG is the biopotential validated by doctors for sleep analysis. On the opposite, CST mounting PPG and accelerometers are most popular option, able to distinguish sleep/wake, but unable to identify the REM stage and not clinically accepted. To improve accuracy of REM staging by wearable technology, it would be desired to consider other markers in addition to HR/HRV and movement, without penalizing cost, comfortability and wearability in comparison to CST.

In this scenario, we propose a wearable device using three QVAR sensors designed for recording three biopotentials: the EOG, the surface EMG (sEMG), and the ECG. The EOG, used to assess rapid eye movements, can be accurately captured from the Fp1 and Fp2 derivations of the 10-20 international system. To assess muscle atonia, the sEMG can be taken from the masseter or mentalis muscles. The ECG, essential to derive HR and HRV, can be recorded using any derivation. The proposed device follows the strategy of comfort adopted by CST, while adding value through the inclusion of EOG and sEMG, at no additional cost. Leveraging the MEMS technology, the QVAR sensors are embedded in accelerometers and are on the market at the same price. Furthermore, the minimal power consumption of a QVAR sensor during recording (27 μW) ensures that the energy expenditure is negligible, thus presenting a cost-effective solution compared to inertial acquisitions.

Our system is contained into an elastic headband, as illustrated in Figure 12. This headband includes a Mini Nucleo L031K6 board by STMicroelectronics, which embeds a Cortex M0 microcontroller, and three QVAR sensors for acquiring the EMG, the ECG, the EOG.

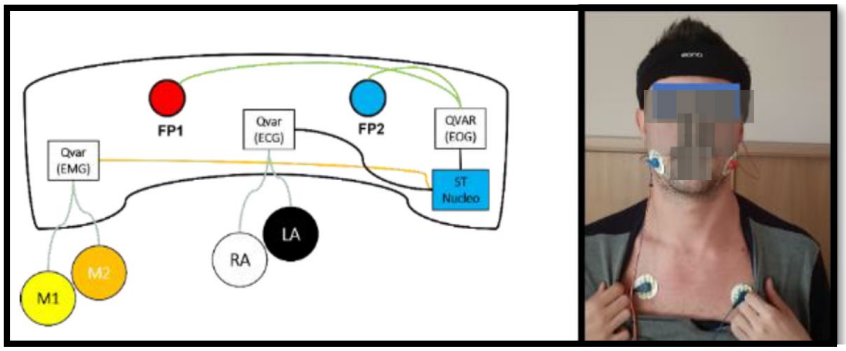

Figure 12. Sketch of the headband for REM sleep analysis, which includes a ST Nucleo board and three QVARs for EMG, ECG, EOG. Electrodes of EMG (M1, M2) and ECG (RA, LL) comes out of the band and are positioned as shown in the photograph. Electrodes of EOG (Fp1, Fp2) are embedded in the band and lye in contact with the forehead skin.

 doi:10.20944/preprints202401.2242.v1

The electrodes on the masseter (M1, M2) for the EMG and the electrodes on the chest (RA, LA) for the ECG are shown in the photograph by the side. Electrodes on the frontal regions (Fp1, Fp2) for the EOG are inside the headband, in contact with the forehead skin. The ECG provides a comprehensive overview of the heart rate which could be also detected through a PPG sensor in order to reduce wiring despite increased power consumption. The QVARs transmit data to the Nucleo through I2C standard. Each QVAR acquires the corresponding biopotential at a sampling frequency of 240 Hz, utilizing a two-electrode configuration. The reference voltage for QVARs is provided by the on-board circuitry, avoiding the third reference electrode.

Tests were performed on a control subject over consecutive nights. A result of main interest is reported in Figure 13. This figure represents a specific 45-minute timeframe during a night, which starts approximately 3 hours after the subject fell asleep. The graphical representation reports the traces of the three biopotentials as a function of time, covering the interval from 3:10 to 3:55 a.m. (in these figures, the time scale has an internal origin). When considering the HR, derived from the trace recorded by QVAR 1, initially HR remains below 55 bpm in the first minutes, then, at 3:28, the HR exhibits a wide variability with bursts reaching up to 80 bpm. This interval of pronounced HRV stops at 3:45, after which HR reverts to values below 55 bpm. The 17-minute interval between 3:28 and 3:45 is highlighted with a grey shadow. Concerning the eye activity, detected by the QVAR 2, the EOG signal remains close to zero for the initial 8 minutes, indicating an absence of eye movements. Then, around 3:28, there is a substantial increase in eye activity, stopping at 3:45. Lastly, regarding the masseter tone detected by the QVAR 3, in the shadowed interval, the masseter manifests a total atonia, while in other intervals a residual constant contraction is present. The *simultaneous* occurrence of all the three patterns was an extraordinary event, presenting only two times throughout the night of testing, with durations of 17 and 15 minutes. On the contrary, in other intervals of variable durations, frequent changes in the individual signals under consideration occurred. In particular, QVAR 1 often recorded pronounced variability of HR, underscoring the limitations of CST in accurately analyzing sleep patterns.

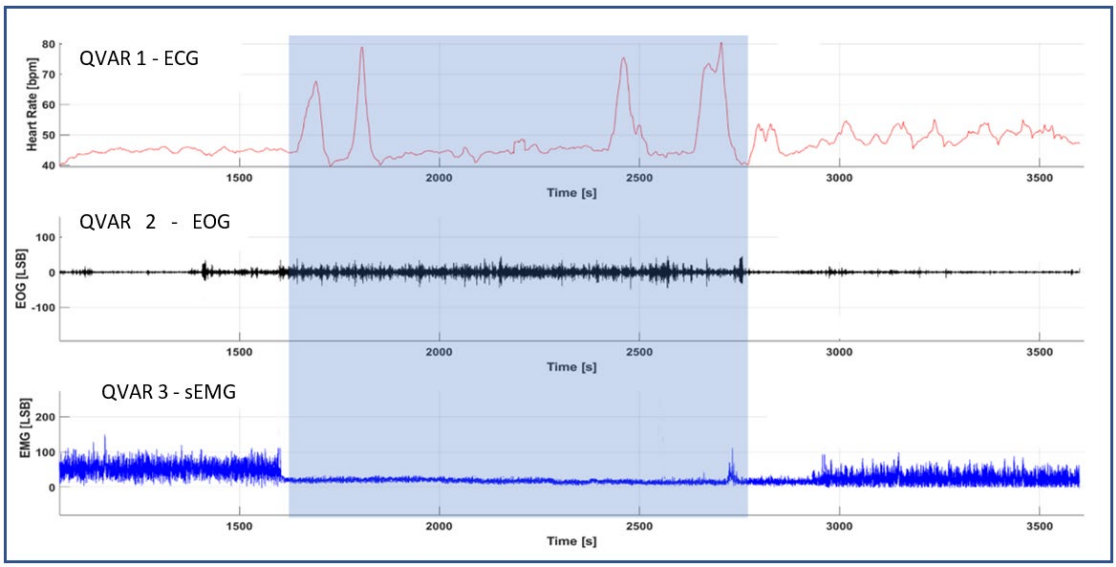

Figure 13. Traces of HR, EOG, sEMG recorded by the three QVARs in a time interval of 45 minutes during the nocturnal test. The 17 minutes long shadowed interval denotes the occurrence of simultaneous alteration of the three biopotentials.

5. Conclusions

We have introduced an innovative methodology for biopotential acquisition based on a commercial MEMS multi-sensor integrated platform mounting electrostatic charge variation (QVAR) sensors. The main advantage of the QVAR sensor is the extremely low-power consumption and its versatility in managing signals of different nature. Indeed, the QVAR sensor was originally intended

for presence tracking in automotive, so the existing setup has been engineered for the acquisition of biopotentials, designing a dedicated front-end and writing a proper firmware. The other MEMS features can enable, as written before, further useful readings without augment cost, power consumption and space. For example, with an accelerometer on the nose it is possible to detect the breathing rate during the sleep and the motion due to obstructive apnea or involuntary movements [72]. To our knowledge, this is the first time that an electrostatic sensor based on electric charge transfer is used for health applications.

Preliminary tests were systematically performed to verify the correct acquisition of biopotentials. To the aim, ECG, EEG, EOG, sEMG traces were recorded on control subjects using simultaneously QVARs and gold standards under the supervision of doctors. The comparison was excellent in all the tests, with no appreciable discrepancy between the two set-ups.

As applications of the QVAR technology for health purposes, we proposed two wearable systems, specifically for nocturnal use in domestic environment. One system records ECG and one-channel EEG for monitoring specific vital signs of diabetic patients before and during nocturnal hypoglycemic crisis. The other system records EOG, ECG and sEMG on the masseter muscle for screening the Rapid-Eye-Movement (REM) sleep phase. In both cases, the nocturnal polygraph recording was successful and the subjects did not report any discomfort.

Clinical considerations are immature and beyond the topic of this paper.

As a conclusion, we can definitely affirm that MEMS QVAR technology provides an incredibly low power, unexplored solution to biopotentials acquisition, and also enables adding this type of functionality to any existing MEMS board at near-zero additional power consumption. For these reasons, those sensors open to additional possibilities for wearable sensing and strengthen the role of MEMS technology in medical wearable applications for long time synchronous acquisition of biopotentials and other physical parameters.

Authors contribution: Conceptualization, Fernanda Irrera, Alessandro Gumiero, Antonio Suppa, Angelo Avogaro; Data curation, Fernanda Irrera, Alessandro Gumiero, Antonio Suppa, Angelo Avogaro; Formal analysis, Fernanda Irrera, Alessandro Gumiero; Investigation, Fernanda Irrera, Alessandro Zampogna, Federico Boscari; Methodology, Fernanda Irrera, Alessandro Gumiero; Project administration, Fernanda Irrera, Luigi Della Torre; Resources, Alessandro Gumiero, Luigi Della Torre, Alessandro Zampogna, Antonio Suppa, Federico Boscari, Angelo Avogaro; Software, Fernanda Irrera; Supervision, Fernanda Irrera, Nicola Picozzi, Alessandro Gumiero, Antonio Suppa, Angelo Avogaro; Validation, Alessandro Zampogna, Nicola Picozzi, Antonio Suppa, Federico Boscari, Angelo Avogaro; Writing – original draft, Fernanda Irrera; Writing – review & editing, Fernanda Irrera, Alessandro Gumiero, Alessandro Zampogna, Federico Boscari, Angelo Avogaro, Luigi Della Torre, Nicola Picozzi, Antonio Suppa.

Acknowledgments: The authors wish to thank the control subjects and the patient for their kind collaboration.

References

1. Zampogna, A.; Mileti, I.; Palermo, E.; Celletti, C.; Paoloni, M.; Manoni, A.; Mazzetta, I.; Dalla Costa, G.; Pérez-López, C.; Camerota, F.; et al. Fifteen Years of Wireless Sensors for Balance Assessment in Neurological Disorders. Sensors 2020, 20, 3247, doi:10.3390/s20113247.
2. Jani, A.B.; Bagree, R.; Roy, A.K. Design of a Low-Power, Low-Cost ECG Amp; EMG Sensor for Wearable Biometric and Medical Application. In Proceedings of the 2017 IEEE SENSORS; October 2017; pp. 1–3.
3. Mazzetta, I.; Zampogna, A.; Suppa, A.; Gumiero, A.; Pessione, M.; Irrera, F. Wearable Sensors System for an Improved Analysis of Freezing of Gait in Parkinson's Disease Using Electromyography and Inertial Signals. Sensors 2019, 19, 948.
4. Mai, N.-D.; Hoang Long, N.M.; Chung, W.-Y. 1D-CNN-Based BCI System for Detecting Emotional States Using a Wireless and Wearable 8-Channel Custom-Designed EEG Headset. In Proceedings of the 2021 IEEE International Conference on Flexible and Printable Sensors and Systems (FLEPS); June 2021; pp. 1–4.
5. Ogino, M.; Kanoga, S.; Muto, M.; Mitsukura, Y. Analysis of Prefrontal Single-Channel EEG Data for Portable Auditory ERP-Based Brain–Computer Interfaces. Frontiers in Human Neuroscience 2019, 13.
6. Hughes, J.R.; Zialcita, M.L. EEG in the Elderly: Seizures vs. Syncope. Clinical Electroencephalography 2000, 31, 131–137, doi:10.1177/155005940003100305.

7. Livia Fantini, M.; Gagnon, J.-F.; Petit, D.; Rompré, S.; Décary, A.; Carrier, J.; Montplaisir, J. Slowing of Electroencephalogram in Rapid Eye Movement Sleep Behavior Disorder: Electroencephalogram in RBD. Ann Neurol. 2003, 53, 774–780, doi:10.1002/ana.10547.
8. Diadem Available online: https://www.bitbrain.com/neurotechnology-products/dry-eeg/diadem (accessed on 13 December 2021).
9. BrainBit Available online: http://brainbit.com/ (accessed on 13 December 2021).
10. Dry EEG Headsets | Products | CGX Available online: https://www.cgxsystems.com/products (accessed on 13 December 2021).
11. Li, D.; Puglia, M.P.; Lapointe, A.P.; Ip, K.I.; Zierau, M.; McKinney, A.; Vlisides, P.E. Age-Related Changes in Cortical Connectivity During Surgical Anesthesia. Frontiers in Aging Neuroscience 2020, 11, 371, doi:10.3389/fnagi.2019.00371.
12. Miller, S.; Chelian, S.; Mcburnett, W.; Tsou, W.; Kruse, A. An Investigation of Computer-Based Brain Training on the Cognitive and EEG Performance of Employees.; July 24 2019; Vol. 2019.
13. Kim, H.; Yoshimura, N.; Koike, Y. Classification of Movement Intention Using Independent Components of Premovement EEG. Frontiers in Human Neuroscience 2019, 13, 63, doi:10.3389/fnhum.2019.00063.
14. DSI 7 Flex Available online: https://wearablesensing.com/products/dsi-7-flex/ (accessed on 13 December 2021).
15. Product Available online: https://mentalab.com/product (accessed on 2 February 2022).
16. Apicella, A.; Arpaia, P.; Mastrati, G.; Moccaldi, N. High-Wearable EEG-Based Detection of Emotional Valence for Scientific Measurement of Emotions; 2021;
17. Nakamura, T.; Alqurashi, Y.D.; Morrell, M.J.; Mandic, D.P. Hearables: Automatic Overnight Sleep Monitoring With Standardized In-Ear EEG Sensor. IEEE Transactions on Biomedical Engineering 2020, 67, 203–212, doi:10.1109/TBME.2019.2911423.
18. Hölle, D.; Meekes, J.; Bleichner, M.G. Mobile Ear-EEG to Study Auditory Attention in Everyday Life. Behav Res 2021, 53, 2025–2036, doi:10.3758/s13428-021-01538-0.
19. Steinberg, C.; Bennett, M.T.; Krahn, A.D. Extended ECG Monitoring. In Cardiac Arrhythmias, Pacing and Sudden Death; Kowey, P., Piccini, J.P., Naccarelli, G., Reiffel, J.A., Eds.; Cardiovascular Medicine; Springer International Publishing: Cham, 2017; pp. 49–60 ISBN 978-3-319-58000-5.
20. Bulková, V. Long-Term ECG Monitoring. Vnitr Lek 2021, 67, 16–21.
21. Bender, E. Prolonged Holter-ECG Monitoring Found to Improve Detection of Atrial Fibrillation After Acute Stroke. Neurology Today 2017, 17, 8, doi:10.1097/01.NT.0000516802.99234.ed.
22. Bayoumy, K.; Gaber, M.; Elshafeey, A.; Mhaimeed, O.; Dineen, E.H.; Marvel, F.A.; Martin, S.S.; Muse, E.D.; Turakhia, M.P.; Tarakji, K.G.; et al. Smart Wearable Devices in Cardiovascular Care: Where We Are and How to Move Forward. Nat Rev Cardiol 2021, 18, 581–599, doi:10.1038/s41569-021-00522-7.
23. D. Brunelli, A. M. Tadesse, B. Vodermayer, M. Nowak and C. Castellini, Low-cost wearable multichannel surface EMG acquisition for prosthetic hand control. 6th International Workshop on Advances in Sensors and Interfaces (IWASI), Gallipoli, Italy, 2015, pp. 94-99, 10.1109/IWASI.2015.7184964.
24. F. Yinfeng, L. Honghai, L. Gongfa, Z. Xiangyang, A Multichannel Surface EMG System for Hand Motion Recognition. International Journal of Humanoid Robotics 2015, Volume 12, No. 2, pp. 1-13, 10.1142/S0219843615500115
25. MYO Armband: https://www.myo.com
26. Liu, Y.; Huang, H. Towards a high-stability EMG recognition system for prosthesis control: A one-class classification based non-target EMG pattern filtering scheme. In Proceedings of the 2009 IEEE International Conference on Systems, Man and Cybernetics, San Antonio, TX, USA, 11–14 October 2009; pp. 4752–4757.
27. Huang, P.; Wang, H.; Wang, Y.; Liu, Z.; Samuel, O.W.; Yu, M.; Li, X.; Chen, S.; Li, G. Identification of Upper-Limb Movements Based on Muscle Shape Change Signals for Human-Robot Interaction. Comput. Math. Methods Med. 2020, 2020, 1–14. [Google Scholar]
28. Su, Y.; Fisher, M.H.; Wolczowski, A.; Bell, G.D.; Burn, D.; Gao, R. Towards an EMG Controlled Prosthetic Hand Using a 3D Electromagnetic Positioning System. In Proceedings of the 2005 IEEE Instrumentationand Measurement Technology Conference Proceedings, Ottawa, ON, Canada, 16–19 May 2005; pp. 261–266.
29. Trignotm Wireless Biofeedback System User's Guide Delsys Incorporated. 2021. Available online: https://www.delsys.com/downloads/USERSGUIDE/trigno/wireless-biofeedback-system.pdf.
30. Mini Wave Infinity. 2004. Available online:http://www.h-elmar-ms.pl/helmar-ms/plik/cometa-systems_wavetrack-inertial-system_nn4776.pdf.

31. Ultium EMG Brochure. 2019. Available online:https://www.noraxo-n.com/noraxon-download/ultium-emg-datasheet/.
32. Shimmer User Manual Revision 3p. 2017. Available online: http://www.shimmersensing.com/images/uploads/docs/Shimmer_User_Manual_rev3p.pdf.
33. Yi-Da Wu, Shanq-Jang Ruan, Yu-Hao Lee B*iosensors* 2021, *11*(11), 411; An Ultra-Low Power Surface EMG Sensor for Wearable Biometric and Medical Applications https://doi.org/10.3390/bios11110411
34. Casson, A.J. Wearable EEG and Beyond. Biomed Eng Lett 2019, 9, 53–71, doi:10.1007/s13534-018-00093-6
35. Roy, S.K.; Shah, S.U.; Villa-Lopez, E.; Murillo, M.; Arenas, N.; Oshima, K.; Chang, R.-K.; Lauzon, M.; Guo, X.; Pillutla, P. Comparison of Electrocardiogram Quality and Clinical Interpretations Using Prepositioned ECG Electrodes and Conventional Individual Electrodes. Journal of Electrocardiology 2020, 59, 126–133, doi:10.1016/j.jelectrocard.2020.02.005.
36. Manoni, A.; Gumiero, A.; Zampogna, A.; Ciarlo, C.; Panetta, L.; Suppa, A.; Della Torre, L.; Irrera, F.; Long-Term Polygraphic Monitoring through MEMS and Charge Transfer for Low-Power Wearable Applications. Sensors (Basel). 2022 Mar 27;22(7):2566. doi: 10.3390/s22072566.
37. Hossain, M.B.; Bashar, S.K.; Walkey, A.J.; McManus, D.D.; Chon, K.H. An Accurate QRS Complex and P Wave Detection in ECG Signals Using Complete Ensemble Empirical Mode Decomposition with Adaptive Noise Approach. IEEE Access 2019, 7, 128869–128880, doi:10.1109/ACCESS.2019.2939943.
38. Cai, Z.; Li, J.; Zhang, X.; Shen, Q.; Murray, A.; Liu, C. How Accurate Are ECG Parameters from Wearable Single-Lead ECG System for 24-Hours Monitoring. In Proceedings of the 2019 Computing in Cardiology (CinC); September 2019; p. Page 1-Page 4.
39. Witvliet, M.P.; Karregat, E.P.M.; Himmelreich, J.C.L.; de Jong, J.S.S.G.; Lucassen, W.A.M.; Harskamp, R.E. Usefulness, Pitfalls and Interpretation of Handheld Single-lead Electrocardiograms. Journal of Electrocardiology 2021, 66, 33–37, doi:10.1016/j.jelectrocard.2021.02.011.
40. Jurcak, V.; Tsuzuki, D.; Dan, I. 10/20, 10/10, and 10/5 Systems Revisited: Their Validity as Relative Head-Surface-Based Positioning Systems. Neuroimage 2007, 34, 1600–1611, doi:10.1016/j.neuroimage.2006.09.024
41. Zeng, H.; Song, A.; Yan, R.; Qin, H. EOG Artifact Correction from EEG Recording Using Stationary Subspace Analysis and Empirical Mode Decomposition. Sensors (Basel) 2013, 13, 14839–14859, doi:10.3390/s131114839.
42. Belkhiria, C.; Peysakhovich, V. Electro-Encephalography and Electro-Oculography in Aeronautics: A Review Over the Last Decade (2010–2020). Frontiers in Neuroergonomics 2020, 1, 3, doi:10.3389/fnrgo.2020.606719.
43. Creel, D.J. The Electrooculogram. Handb Clin Neurol 2019, 160, 495–499, doi:10.1016/B978-0-444-64032-1.00033-3.
44. Peever, J.; Fuller, P.M. The Biology of REM Sleep. Current Biology 2017, 27, R1237–R1248, doi:10.1016/j.cub.2017.10.026.
45. D. Artanto, M. P. Sulistyanto, I. D. Pranowo and E. E. Pramesta, Drowsiness detection system based on eye-closure using a low-cost EMG and ESP8266. 2nd International conferences on Information Technology, Information Systems and Electrical Engineering (ICITISEE), Yogyakarta, Indonesia, 2017, pp. 235-238, 10.1109/ICITISEE.2017.8285502.
46. S. Shin, Y. Baek, J. Lee, Y. Eun and S. H. Son, Korean sign language recognition using EMG and IMU sensors based on group-dependent NN models. IEEE Symposium Series on Computational Intelligence (SSCI), Honolulu, HI, USA, 2017, pp. 1-7, 10.1109/SSCI.2017.8280908.
47. Yamaguchi, T., Mikami, S., Saito, M., Okada, K., Gotouda, A., Newly developed ultraminiature wearable electromyogram system useful for analyses of masseteric activity during the whole day, Journal of Prosthodontic Research 2018, Volume 62, Issue 1, pp. 110-115, 10.1016/j.jpor.2017.04.001.
48. A. Gruebler and K. Suzuki, Design of a Wearable Device for Reading Positive Expressions from Facial EMG Signals. in IEEE Transactions on Affective Computing 2014, vol. 5, no. 3, pp. 227-237, 10.1109/TAFFC.2014.2313557.
49. https://www.mikroe.com/emg-click
50. T. Yosef, "Hypoglycemia Among Type 1 Diabetes Patients After Insulin Use in Southwest Ethiopia," Front. Endocrinol., vol. 12, p. 684570, Oct. 2021, doi: 10.3389/fendo.2021.684570.
51. R. J. McCrimmon and R. S. Sherwin, "Hypoglycemia in Type 1 Diabetes," Diabetes, vol. 59, no. 10, pp. 2333–2339, Oct. 2010, doi: 10.2337/db10-0103.

52. P. Loumpardia and M. S.B. Huda, "Symptoms of Hypoglycaemia," in Blood Glucose Levels, L. Szablewski, Ed. IntechOpen, 2020. doi: 10.5772/intechopen.88674.
53. J. L. B. Marques et al., "Altered ventricular repolarization during hypoglycaemia in patients with diabetes," Diabet. Med., vol. 14, no. 8, pp. 648–654, Aug. 1997, doi: 10.1002/(SICI)1096-9136(199708)14:8<648::AID-DIA418>3.0.CO;2-1.
54. E. M. Kallergis, C. A. Goudis, E. N. Simantirakis, G. E. Kochiadakis, and P. E. Vardas, "Mechanisms, Risk Factors, and Management of Acquired Long QT Syndrome: A Comprehensive Review," The Scientific World Journal, vol. 2012, pp. 1–8, 2012, doi: 10.1100/2012/212178.
55. S. Bachmann et al., "Autonomic cardiac regulation during spontaneous nocturnal hypoglycemia in children with type 1 diabetes," Pediatric Diabetes, vol. 22, no. 7, pp. 1023–1030, Nov. 2021, doi: 10.1111/pedi.13262.
56. M. Mylona, S. Liatis, G. Anastasiadis, C. Kapelios, and A. Kokkinos, "Severe iatrogenic hypoglycaemia requiring medical assistance is associated with concurrent prolongation of the QTc interval," Diabetes Research and Clinical Practice, vol. 161, p. 108038, Mar. 2020, doi: 10.1016/j.diabres.2020.108038.
57. O. Diouri et al., "Hypoglycaemia detection and prediction techniques: A systematic review on the latest developments," Diabetes Metabolism Res, vol. 37, no. 7, Oct. 2021, doi: 10.1002/dmrr.3449.
58. O. Elvebakk et al., "A multiparameter model for non-invasive detection of hypoglycemia," Physiol. Meas., vol. 40, no. 8, p. 085004, Sep. 2019, doi: 10.1088/1361-6579/ab3676.
59. M. Porumb, S. Stranges, A. Pescapè, and L. Pecchia, "Precision Medicine and Artificial Intelligence: A Pilot Study on Deep Learning for Hypoglycemic Events Detection based on ECG," Sci Rep, vol. 10, no. 1, p. 170, Jan. 2020, doi: 10.1038/s41598-019-56927-5.
60. M. Olde Bekkink, M. Koeneman, B. E. de Galan, and S. J. Bredie, "Early Detection of Hypoglycemia in Type 1 Diabetes Using Heart Rate Variability Measured by a Wearable Device," Diabetes Care, vol. 42, no. 4, pp. 689–692, Apr. 2019, doi: 10.2337/dc18-1843.
61. C. J. Hsu and S. T. Chen, "IDF21-0409 Hypoglycemia and heart rate variability: synchronous detection by Holter and continuous glucose monitors," Diabetes Research and Clinical Practice, vol. 186, p. 109534, Apr. 2022, doi: 10.1016/j.diabres.2022.109534.
62. C. Q. Ngo, R. Chai, T. V. Nguyen, T. W. Jones, e H. T. Nguyen, «Nocturnal Hypoglycemia Detection using EEG Spectral Moments under Natural Occurrence Conditions», in 2019 41st Annual International Conference of the IEEE Engineering in Medicine and Biology Society (EMBC), Berlin, Germany, lug. 2019, pp. 7177–7180. doi: 10.1109/EMBC.2019.8856695.
63. C. Q. Ngo, R. Chai, T. V. Nguyen, T. W. Jones, e H. T. Nguyen, «Electroencephalogram Spectral Moments for the Detection of Nocturnal Hypoglycemia», IEEE J. Biomed. Health Inform., vol. 24, fasc. 5, pp. 1237–1245, mag. 2020, doi: 10.1109/JBHI.2019.2931782.
64. C. Q. Ngo, R. Chai, T. W. Jones, e H. T. Nguyen, «The Effect of Hypoglycemia on Spectral Moments in EEG Epochs of Different Durations in Type 1 Diabetes Patients», IEEE J. Biomed. Health Inform., vol. 25, fasc. 8, pp. 2857–2865, ago. 2021, doi: 10.1109/JBHI.2021.3054876.
65. Sateia, M.J. International Classification of Sleep Disorders-Third Edition. Chest 2014, 146, 1387–1394, doi:10.1378/chest.14-0970.
66. Gorantla, S.; Rodriguez, C.L. The Diagnostic Challenge of Dream-Enactment Behaviors. Journal of Clinical Sleep Medicine 2020, 16, 1837–1838, doi:10.5664/jcsm.8848.
67. Masi,G; Ampriamo,G; Priano, L.; Ferraris, C. *Electronics* 2023, *12*(5), 1098, doi: 10.3390/electronics 12051098
68. Korotun, M.; Quintero, L.; Hahn, S.S. Rapid Eye Movement Behavior Disorder and Other Parasomnias. Clinics in Geriatric Medicine 2021, 37, 483–490, doi:10.1016/j.cger.2021.04.008.
69. Mieno, Y.; Hayashi, M.; Hirochi, M.; Ikeda, A.; Kako, H.; Ina, T.; Maeda, Y.; Maeda, S.; Inoue, T.; Souma, T.; et al. Availability of Home Sleep Apnea Test Equipment LS-140 on a Comparison with Polysomnography. Fujita Med J 2022, 8, 17–24, doi:10.20407/fmj.2020-014.
70. White, C.; Hill, E.A.; Morrison, I.; Riha, R.L. Diagnostic Delay in REM Sleep Behavior Disorder (RBD). J Clin Sleep Med 2012, 8, 133–136, doi:10.5664/jcsm.1762.
71. Postuma, R.B.; Gagnon, J.-F.; Montplaisir, J.Y. REM Sleep Behavior Disorder: From Dreams to Neurodegeneration. Neurobiology of Disease 2012, 46, 553–558, doi:10.1016/j.nbd.2011.10.003.
72. Manoni, A.; Loreti, F.; Radicioni, V.; Pellegrino, D.; Torre, L.D.; Gumiero, A.; Halicki, D.; Palange, P.; Irrera, F. A New Wearable System for Home Sleep Apnea Testing, Screening, and Classification. Sensors 2020, 20, 7014, doi:10.3390/s20247014.

73. Arulvallal, S.; U., S.; T., R. Design and Development of Wearable Device for Continuous Monitoring of Sleep APNEA Disorder. In Proceedings of the 2019 International Conference on Communication and Signal Processing (ICCSP); April 2019; pp. 0050–0053.
74. Sarmiento, K.F.; Folmer, R.L.; Stepnowsky, C.J.; Whooley, M.A.; Boudreau, E.A.; Kuna, S.T.; Atwood, C.W.; Smith, C.J.; Yarbrough, W.C. National Expansion of Sleep Telemedicine for Veterans: The TeleSleep Program. J Clin Sleep Med 2019, 15, 1355–1364, doi:10.5664/jcsm.7934.
75. Hwang, D.; Chang, J.W.; Benjafield, A.V.; Crocker, M.E.; Kelly, C.; Becker, K.A.; Kim, J.B.; Woodrum, R.R.; Liang, J.; Derose, S.F. Effect of Telemedicine Education and Telemonitoring on Continuous Positive Airway Pressure Adherence. The Tele-OSA Randomized Trial. Am J Respir Crit Care Med 2018, 197, 117–126, doi:10.1164/rccm.201703-0582OC.
76. Rb, B.; R., Brooks; C.E., Gamaldo; S.M., Harding AASM Scoring Manual Version 2.2. 2015, 7.
77. Kanady, J.C.; Drummond, S.P.A.; Mednick, S.C. Actigraphic Assessment of a Polysomnographic-Recorded Nap: A Validation Study. Journal of Sleep Research 2011, 20, 214–222, doi:10.1111/j.1365-2869.2010.00858.x.
78. Kosmadopoulos, A.; Sargent, C.; Darwent, D.; Zhou, X.; Roach, G.D. Alternatives to Polysomnography (PSG): A Validation of Wrist Actigraphy and a Partial-PSG System. Behav Res 2014, 46, 1032–1041, doi:10.3758/s13428-013-0438-7.
79. Long, X.; Fonseca, P.; Foussier, J.; Haakma, R.; Aarts, R.M. Sleep and Wake Classification With Actigraphy and Respiratory Effort Using Dynamic Warping. IEEE Journal of Biomedical and Health Informatics 2014, 18, 1272–1284, doi:10.1109/JBHI.2013.2284610.
80. Assessing Sleep Using Hip and Wrist Actigraphy - Slater - 2015 - Sleep and Biological Rhythms - Wiley Online Library Available online: https://onlinelibrary.wiley.com/doi/abs/10.1111/sbr.12103 (accessed on 28 September 2022).
81. Kagawa, M.; Suzumura, K.; Matsui, T. Sleep Stage Classification by Non-Contact Vital Signs Indices Using Doppler Radar Sensors. In Proceedings of the 2016 38th Annual International Conference of the IEEE Engin. in Medicine and Biology Society (EMBC), 2016, pp. 4913–16.
82. Ye, Y.; Yang, K.; Jiang, J.; Ge, B. Automatic Sleep and Wake Classifier with Heart Rate and Pulse Oximetry: Derived Dynamic Time Warping Features and Logistic Model. In Proceedings of the 2016 Annual IEEE Systems Conference (SysCon); April 2016; pp. 1–6.
83. Osterbauer, B.; A. Koempel, J.; L. Davidson Ward, S.; M. Fisher, L.; M. Don, D. A Comparison Study Of The Fitbit Activity Monitor And PSG For Assessing Sleep Patterns And Movement In Children. JOA 2016, 1, 24–35, doi:10.14302/issn.2379-8572.joa-15-891.
84. Chinoy, E.D.; Cuellar, J.A.; Jameson, J.T.; Markwald, R.R. <p>Performance of Four Commercial Wearable Sleep-Tracking Devices Tested Under Unrestricted Conditions at Home in Healthy Young Adults</P>. NSS 2022, 14, 493–516, doi:10.2147/NSS.S348795.
85. Stone, J.D.; Rentz, L.E.; Forsey, J.; Ramadan, J.; Markwald, R.R.; Finomore, V.S.; Galster, S.M.; Rezai, A.; Hagen, J.A. Evaluations of Commercial Sleep Technologies for Objective Monitoring During Routine Sleeping Conditions. Nat Sci Sleep 2020, 12, 821–842, doi:10.2147/NSS.S270705.
86. de Zambotti, M.; Cellini, N.; Goldstone, A.; Colrain, I.M.; Baker, F.C. Wearable Sleep Technology in Clinical and Research Settings. Med Sci Sports Exerc 2019, 51, 1538–1557, doi:10.1249/MSS.1947.
87. Gavriloff, D.; Sheaves, B.; Juss, A.; Espie, C.A.; Miller, C.B.; Kyle, S.D. Sham Sleep Feedback Delivered via Actigraphy Biases Daytime Symptom Reports in People with Insomnia: Implications for Insomnia Disorder and Wearable Devices. J Sleep Res 2018, 27, e12726, doi:10.1111/jsr.12726.
88. Imtiaz, S.A. A Systematic Review of Sensing Technologies for Wearable Sleep Staging. Sensors 2021, 21, 1562, doi:10.3390/s21051562.
89. Wulterkens, B.M.; Fonseca, P.; Hermans, L.W.; Ross, M.; Cerny, A.; Anderer, P.; Long, X.; Dijk, J.P. van; Vandenbussche, N.; Pillen, S.; et al. It Is All in the Wrist: Wearable Sleep Staging in a Clinical Population versus Reference Polysomnography</P>. NSS 2021, 13, 885–897, doi:10.2147/NSS.S306808.
90. Fonseca, P.; van Gilst, M.M.; Radha, M.; Ross, M.; Moreau, A.; Cerny, A.; Anderer, P.; Long, X.; van Dijk, J.P.; Overeem, S. Automatic Sleep Staging Using Heart Rate Variability, Body Movements, and Recurrent Neural Networks in a Sleep Disordered Population. Sleep 2020, 43, zsaa048, doi:10.1093/sleep/zsaa048.
91. Korkalainen, H.; Aakko, J.; Duce, B.; Kainulainen, S.; Leino, A.; Nikkonen, S.; Afara, I.O.; Myllymaa, S.; Töyräs, J.; Leppänen, T. Deep Learning Enables Sleep Staging from Photoplethysmogram for Patients with Suspected Sleep Apnea. Sleep 2020, 43, zsaa098, doi:10.1093/sleep/zsaa098.

92. Yuda, E.; Yoshida, Y.; Sasanabe, R.; Tanaka, H.; Shiomi, T.; Hayano, J. Sleep Stage Classification by a Combination of Actigraphic and Heart Rate Signals. Journal of Low Power Electronics and Applications 2017, 7, 28, doi:10.3390/jlpea7040028.